6-20-2011

Propagation Of Solar Energetic Particles In Three-Dimensional Interplanetary Magnetic Fields: In View Of Characteristics Of Sources

H. Q. He

Gang Qin

Ming Zhang

The Astrophysical Journal, 734:74 (11pp), 2011 June 20 doi:10.1088/0004-637X/734/2/74

PROPAGATION OF SOLAR ENERGETIC PARTICLES IN THREE-DIMENSIONAL INTERPLANETARY MAGNETIC FIELDS: IN VIEW OF CHARACTERISTICS OF SOURCES

H.-Q. He[1,2], G. Qin[1], and M. Zhang[3]
[1] State Key Laboratory of Space Weather, Center for Space Science and Applied Research, Chinese Academy of Sciences, Beijing 100190, China; hqhe@spaceweather.ac.cn, gqin@spaceweather.ac.cn
[2] College of Earth Sciences, Graduate University of Chinese Academy of Sciences, Beijing 100049, China
[3] Department of Physics and Space Science, Florida Institute of Technology, Melbourne, FL 32901, USA; mzhang@fit.edu
Received 2010 November 11; accepted 2011 April 4; published 2011 May 26

ABSTRACT

In this paper, a model of solar energetic particle (SEP) propagation in the three-dimensional Parker interplanetary magnetic field is calculated numerically. We study the effects of the different aspects of particle sources on the solar surface, which include the source location, coverage of latitude and longitude, and spatial distribution of source particle intensity, on propagation of SEPs with both parallel and perpendicular diffusion. We compute the particle flux and anisotropy profiles at different observation locations in the heliosphere. From our calculations, we find that the observation location relative to the latitudinal and longitudinal coverage of particle source has the strongest effects on particle flux and anisotropy profiles observed by a spacecraft. When a spacecraft is directly connected to the solar sources by the interplanetary magnetic field lines, the observed particle fluxes are larger than when the spacecraft is not directly connected. This paper focuses on the situations when a spacecraft is not connected to the particle sources on the solar surface. We find that when the magnetic footpoint of the spacecraft is farther away from the source, the observed particle flux is smaller and its onset and maximum intensity occur later. When the particle source covers a larger range of latitude and longitude, the observed particle flux is larger and appears earlier. There is east–west azimuthal asymmetry in SEP profiles even when the source distribution is east–west symmetric. However, the detail of particle spatial distribution inside the source does not affect the profile of the SEP flux very much. When the magnetic footpoint of the spacecraft is significantly far away from the particle source, the anisotropy of particles in the early stage of an SEP event points toward the Sun, which indicates that the first arriving particles come from outside of the observer through perpendicular diffusion at large radial distances.

Key words: interplanetary medium – magnetic fields – solar–terrestrial relations – Sun: coronal mass ejections (CMEs) – Sun: flares – Sun: particle emission

1. INTRODUCTION

Solar energetic particles (SEPs) are produced and released from the Sun with limited sizes and at various locations relative to the magnetic field line connecting to the observer, and are transported throughout the interplanetary field (IMF) with fluctuations. Impulsive SEP events are related to solar flares, which have small sizes. Even coronal mass ejections (CMEs) are limited, too. Reames (1999) showed some observations of longitudinal effects on SEPs' transport processes. They found that the spiral pattern of the interplanetary magnetic field (Parker 1963) causes an asymmetry in the intensity-time profiles of SEP events from the eastern and western longitudes on the Sun. Cane et al. (1988) studied profiles of 235 intense proton events accumulated over ∼20 years to systematically document the longitude-dependent profiles. Therefore, we need to study how the relative location and size affect SEP profiles. Parker (1963), Roelof (1969), and Earl (1976) introduced a model of SEPs with focused transport equation. Droge (1994) discussed the relation of transport parameters to the structure of the interplanetary magnetic field, with special emphasis on comparison of particle mean free paths determined from fits to intensity and anisotropy profiles with theoretical predictions. Ruffolo (1995) and Qin et al. (2006) found that including adiabatic deceleration can increase the decay rate of the intensity time profile. Zank et al. (2000) and Li et al. (2003) provided a dynamical time-dependent model of particle acceleration at a propagating, evolving interplanetary shock. Qin et al. (2005) showed that the different values of the mean free path for the same SEP event are due to the high anisotropy of the SEPs. These approaches have significantly advanced the understanding of SEPs' transport in interplanetary space. Basically, however, all of these studies only considered particle transport along the averaged interplanetary magnetic field lines. Applications of these models to observations are based on the assumption that SEP events have a spherically symmetric configuration.

According to the quasi-linear theory for cosmic ray diffusion (Jokipii 1966), a perpendicular diffusion coefficient is usually much smaller than a parallel diffusion coefficient. So, the perpendicular diffusion coefficient was ignored in previous studies of SEP transport in interplanetary space. However, Dwyer et al. (1997) and Zhang et al. (2003) reported that the perpendicular diffusion could be comparable to the parallel diffusion. Furthermore, test particle simulations show results contrary to previous theoretical results (e.g., Qin 2002; Qin et al. 2002). In addition, Matthaeus et al. (2003), Shalchi et al. (2004), and Qin (2007) developed theories with nonlinear effects of magnetic fluctuations to agree with simulation results.

SEPs are often observed to form a nearly uniform particle reservoir in the entire inner heliosphere (McKibben 1972; Roelof et al. 1992; Reames et al. 1997; Maclennan et al. 2001; McKibben et al. 2003; Lario et al. 2003). Two different mechanisms have been proposed for the SEP reservoir phenomenon. McKibben (1972) and McKibben et al. (2003) discussed an effective cross-field diffusion to distribute the SEPs uniformly, while Roelof et al. (1992), Reames et al. (1997), and Tan et al. (2009) introduced a diffusion barrier or a reflecting boundary to contain the SEPs long enough for them to be distributed

uniformly through normal diffusion and adiabatic cooling. Lario et al. (2003) discussed the formation of the reservoirs in terms of both fresh injections of SEPs and the formation of compressed magnetic field regions in the heliosphere beyond the Earth orbit (~2–5 AU). Zhang et al. (2009) presented a complete model calculation of SEP transport in a three-dimensional Parker IMF with the effect of magnetic fluctuations. They found that the observed SEP reservoir phenomenon is a robust result of SEP propagation with enhanced "communication" across latitude and longitude.

In previous studies of SEPs' transport in interplanetary space, it is usually assumed that the source particle strength on the Sun is uniform over all the solar longitudes and latitudes. So the effects of individual particle sources on SEPs' transport are ignored. However, as we know from observational and theoretical results, the realistic characteristics (e.g., location, coverage, and spatial variation) of particle sources may differ significantly from each other. For example, the effect of spatial variation in the acceleration region on remote particle observations is a very interesting topic in the community. Giacalone & Neugebauer (2008) suggested that shock-accelerated energetic particle spectrum downstream of a shock may be independent of location along the shock front. Hurford et al. (2006) studied the gamma-ray imaging of solar flares to show that SEPs that produce gamma ray might be accelerated locally by the flare instead of the associated fast CME shock. It is interesting to find out how these characteristics of particle sources affect SEPs' transport processes in the interplanetary space, especially in influencing the time profiles of the flux and anisotropy of SEPs. Therefore, to achieve a more complete understanding of SEPs' transport, it is necessary to investigate the effects of particle sources on the propagation of SEPs in the three-dimensional IMF.

In this paper, we study the effects of particle sources on the propagation of SEPs in the three-dimensional IMF. Generally speaking, the characteristics of particle sources may include the source location, coverage of latitude and longitude, and spatial distribution of source particle intensity. In Section 2, we describe the SEP transport model we use to compute the particle flux as observed by an observer at any position in the heliosphere. In Section 3, we look at how the distribution of particle source with a limited longitude and latitude coverage will affect the time profiles of SEP flux and anisotropy observed on field lines with various magnetic connectivity to the particle source on the Sun. Some possible generalizations of our results will be discussed in Section 4.

2. MODEL

In our model, the focused transport equation that governs the gyrophase-averaged distribution function $f(\mathbf{x}, \mu, p, t)$ of SEPs is written as (e.g., Skilling 1971; Schlickeiser 2002; Qin et al. 2004; Zhang et al. 2009)

$$\frac{\partial f}{\partial t} + \mu v \frac{\partial f}{\partial z} + \mathbf{V}^{\rm sw} \cdot \nabla f + \frac{dp}{dt}\frac{\partial f}{\partial p} + \frac{d\mu}{dt}\frac{\partial f}{\partial \mu} - \frac{\partial}{\partial \mu}\left(D_{\mu\mu}\frac{\partial f}{\partial \mu}\right) - \frac{\partial}{\partial x}\left(\kappa_{xx}\frac{\partial f}{\partial x}\right) - \frac{\partial}{\partial y}\left(\kappa_{yy}\frac{\partial f}{\partial y}\right) = 0, \quad (1)$$

where $\mathbf{x}$ is the position, with z being the coordinate along the average interplanetary magnetic field of the Parker spiral and x and y being the coordinates in the direction perpendicular to the field, p is the particle momentum, μ is the particle pitch-angle cosine, t is the time, v is the particle speed, $\mathbf{V}^{\rm sw}$ is the solar wind velocity, and κ_{xx} and κ_{yy} are perpendicular diffusion coefficients. The term dp/dt, representing the effect of adiabatic cooling, can be written as (Skilling 1971; Qin et al. 2004, 2006)

$$\frac{dp}{dt} = -p\left[\frac{1-\mu^2}{2}\left(\frac{\partial V_x^{\rm sw}}{\partial x} + \frac{\partial V_y^{\rm sw}}{\partial y}\right) + \mu^2 \frac{\partial V_z^{\rm sw}}{\partial z}\right]. \quad (2)$$

The term $d\mu/dt$, which includes the effects of magnetic focusing and the divergence of solar wind flows, may be written as (e.g., Roelof 1969; Isenberg 1997; Kóta & Jokipii 1997)

$$\frac{d\mu}{dt} = \frac{1-\mu^2}{2}\left[-\frac{v}{B}\frac{\partial B}{\partial z} + \mu\left(\frac{\partial V_x^{\rm sw}}{\partial x} + \frac{\partial V_y^{\rm sw}}{\partial y} - 2\frac{\partial V_z^{\rm sw}}{\partial z}\right)\right] = \frac{1-\mu^2}{2}\left[\frac{v}{L} + \mu\left(\frac{\partial V_x^{\rm sw}}{\partial x} + \frac{\partial V_y^{\rm sw}}{\partial y} - 2\frac{\partial V_z^{\rm sw}}{\partial z}\right)\right], \quad (3)$$

where B is the average Parker interplanetary magnetic field, and the magnetic focusing length L is defined by $L = (\mathbf{z}\cdot\nabla \ln B)^{-1}$. We assume that all particles are injected near the Sun so that the particle distribution function obeys a boundary condition at the source $f_b = Q(\mathbf{x}, p, t)$.

The parallel mean free path $\lambda_\parallel$ under the diffusion approximation for a nearly isotropic pitch-angle distribution can be written as (Jokipii 1966; Hasselmann & Wibberenz 1968, 1970; Earl 1974)

$$\lambda_\parallel = \frac{3v}{8}\int_{-1}^{+1}\frac{(1-\mu^2)^2}{D_{\mu\mu}}d\mu. \quad (4)$$

Generally, the parallel mean free path of a particle propagating in the IMF should be a function of location. For simplicity, we assume that the radial mean free path λ_r is constant so that

$$\lambda_\parallel = \lambda_r/\cos^2\psi, \quad (5)$$

where ψ is the angle between the local magnetic field direction and the radial direction (e.g., Bieber et al. 1994). He & Qin (2011) provided an analytical method to quickly determine SEPs' mean free path for impulsive events, which would be a very useful tool in space weather practice.

We use a form of the pitch-angle diffusion coefficient from Beeck & Wibberenz (1986; Qin et al. 2006)

$$D^r_{\mu\mu} = D_{\mu\mu}/\cos^2\psi = D_0 v R^{-1/3}\{|\mu|^{q-1} + h\}(1-\mu^2), \quad (6)$$

where D_0 is a constant indicating the ratio of the magnetic field fluctuation level relative to the average field strength near the Sun and R is the particle's rigidity. The constant h is needed to simulate the ability to scatter particles through $\mu = 0$. The constant q is related to the power spectrum of the magnetic field turbulence $P_{xx}(k_z) \sim k_z^{-q}$ in the inertial range. In this work, we choose $q = 5/3$ for a typical Kolmogorov spectrum. In order to simulate the nonlinear effect to cause large $D_{\mu\mu}$ at $\mu = 0$ (e.g., Qin & Shalchi 2009), we set a relatively large value of $h = 0.2$. In addition, we assume that the two perpendicular diffusion coefficients, λ_x and λ_y, are the same and independent of μ. In our simulations, we typically use $\lambda_r = 0.3$ AU (corresponding to $\lambda_\parallel = 0.67$ AU at 1 AU) and $\lambda_x = \lambda_y = 0.006$ AU for 50 MeV protons. According to the observations (e.g., Bieber et al. 2004) and theories (e.g., Matthaeus et al. 2003), the ratio of $\lambda_x/\lambda_r = \lambda_y/\lambda_r$, 0.02, is reasonable.

In order to solve the transport Equation (1), we use a time-backward Markov stochastic process method (Zhang 1999; Qin et al. 2006). This method can deal easily with an expanded

source energy spectrum. For a detailed description of this method, please refer to Qin et al. (2006).

The source particles are injected at $r \leqslant 0.05$ AU. Its boundary condition is chosen to have the following form:

$$Q(z \leqslant 0.05 \text{ AU}, E_k, \theta, \phi, t) = \frac{C}{t}\frac{E_k^{-\gamma}}{p^2} \times \exp\left(-\frac{\tau_c}{t} - \frac{t}{\tau_L}\right)\xi(\theta, \phi), \quad (7)$$

where $\xi(\theta, \phi)$ is a function of the heliospheric latitudinal θ and longitudinal ϕ that describes the distribution of SEP source strength, E_k is the source particle's kinetic energy, and τ_c and τ_L indicate the rise and decay timescales of source injection profile, respectively. The time profile is represented by a Reid–Axford profile (Reid 1964). Its spectrum form is a power law as expected from a typical shock acceleration process. In most of our simulations, we assume a distribution that covers a limited range longitude ϕ and latitude θ,

$$\xi(\theta, \phi) = \begin{cases} a_0 a(\theta, \phi) & \text{if } |\theta - \theta_0| \leqslant \Delta\theta \text{ and } |\phi - \phi_0| \leqslant \Delta\phi \\ 0 & \text{otherwise,} \end{cases} \quad (8)$$

where (θ_0, ϕ_0) denotes the heliospheric latitude and longitude at the source center, and the constant a_0 is chosen to normalize the average of $a(\theta, \phi)$ over the latitude and longitude ranges of $[\theta_0 - \Delta\theta : \theta_0 + \Delta\theta]$ and $[\phi_0 - \Delta\phi : \phi_0 + \Delta\phi]$, i.e.,

$$a_0 = \frac{2\Delta\phi\,[\sin(\theta_0 + \Delta\theta) - \sin(\theta_0 - \Delta\theta)]}{\int_{\theta_0-\Delta\theta}^{\theta_0+\Delta\theta} \cos\theta \int_{\phi_0-\Delta\phi}^{\phi_0+\Delta\phi} a(\theta, \phi) d\phi d\theta}, \quad (9)$$

here $\Delta\theta$ and $\Delta\phi$ are the half-widths of SEP sources in latitude θ and longitude ϕ, respectively. Furthermore, in this paper we assume a uniform source inside the source region, i.e., $a(\theta, \phi) = 1$, unless otherwise stated. Typical sizes of SEP sources (expanded flares or CMEs) are tens of degrees wide in longitude and latitude (Hundhausen 1993; Maia et al. 2001; Wang et al. 2006), so in our calculations, we set SEP sources with limited coverages between 30° and 90° in longitude and latitude. There is an outer escape boundary at $r = 50$ AU. Essentially, the outer boundary is not necessary for simulations of SEP events lasting less than 10 days.

We typically set $\tau_c = 0.1$ day and $\tau_L = 0.25$ day. The times are approximately consistent with emissions of X-ray or radio waves during a typical solar event. These parameters may change the rise of SEP flux and the absolute intensity at the maximum SEP flux, but the time profile of a long duration SEP event is not sensitive to these constants. The spectral slope of source particles γ is set to be equal to 3, a value typical of particles accelerated by a moderately strong CME shock.

In order to get enough statistics for the calculation of particle anisotropy down to the level of a few percent, we need to simulate 6×10^7 particles. We do it using a Message Passing Interface parallel code on a super-computer cluster.

The anisotropy A is defined as

$$A = \frac{3\int_{-1}^{1} f(\mu)\mu d\mu}{\int_{-1}^{1} f(\mu) d\mu}, \quad (10)$$

where $f(\mu)$ is the differential direction flux. Furthermore, the unit of omnidirectional flux is usually used as $\text{cm}^{-2}\ \text{sr}^{-1}\ \text{s}^{-1}\ \text{MeV}^{-1}$; however, in this work we use an arbitrary unit for convenience in figures.

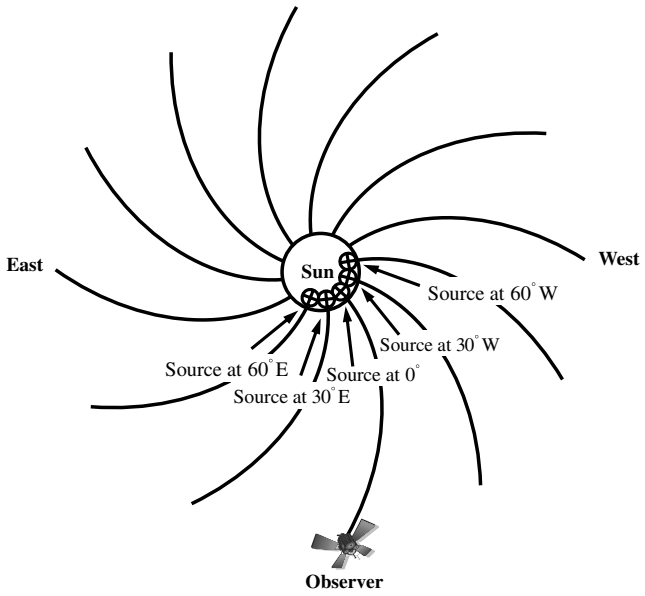

Figure 1. Diagram to show the locations (in longitude) of the particle sources on the Sun relative to the IMF footpoint of the observer (spacecraft). All the five solar sources are located near the equator or at 0° latitude and have a 30° coverage in both latitude and longitude. The observer is also located at 0° latitude.

3. RESULTS

3.1. The Effect of Source Location

Before revealing the results of this part, we present a diagram, i.e., Figure 1, to illustrate the locations (in longitude) of the particle sources on the Sun relative to the IMF footpoint of the observer (spacecraft). In the scenario of this diagram, all the solar sources are located near the equator or 0° latitude and have a 30° coverage in both latitude and longitude. The observer is also located at 0° latitude. Among the five solar sources in the diagram, the middle one's center is connected directly to the observer by IMF, the centers of the two sources on the left are 30° east and 60° east, respectively, away from the IMF footpoint of the observer, whereas the centers of the two sources on the right are 30° west and 60° west, respectively, away from the IMF footpoint of the observer.

Figure 2 shows a comparison of simulations with different source locations relative to the footpoint of the field line connecting the observer. In these simulations, we study 50 MeV protons detected at 1 AU, 0° latitude. The upper and lower panels show the time profile of the SEP omnidirectional flux and anisotropy, respectively. All solar particle sources have the same width, i.e., 30° in longitude and latitude, but their centers are located at various longitudes in the equator. The longitude separations between the sources and the IMF footpoint of the observer are set to be the following values: 0°, 30° west, 30° east, 60° west, and 60° east.

As one can see, when the observer is connected directly to the solar source by IMF, the SEP omnidirectional flux is larger than that otherwise. The farther the IMF footpoint of the observer is away from the source, the smaller is the particle flux observed and also the later the event arrives at the observer's position. The particle fluxes observed are not the same between the sources located east and west from the footpoint of the observer by the same amount of separation in longitude. In particular, the SEP fluxes are larger when the sources are located east of the IMF

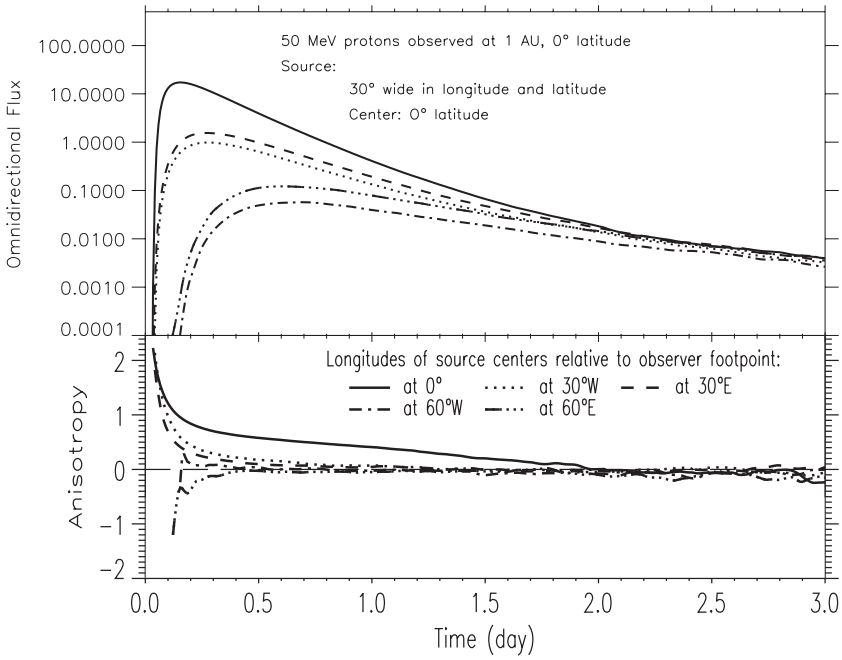

Figure 2. Omnidirectional flux and anisotropy of 50 MeV protons observed at 1 AU, 0° latitude. Different line styles indicate different distances in longitude between the IMF footpoint of the observer and the center of particle sources on the Sun. All the sources are located in the equator or at 0° latitude and have a 30° coverage in both latitude and longitude.

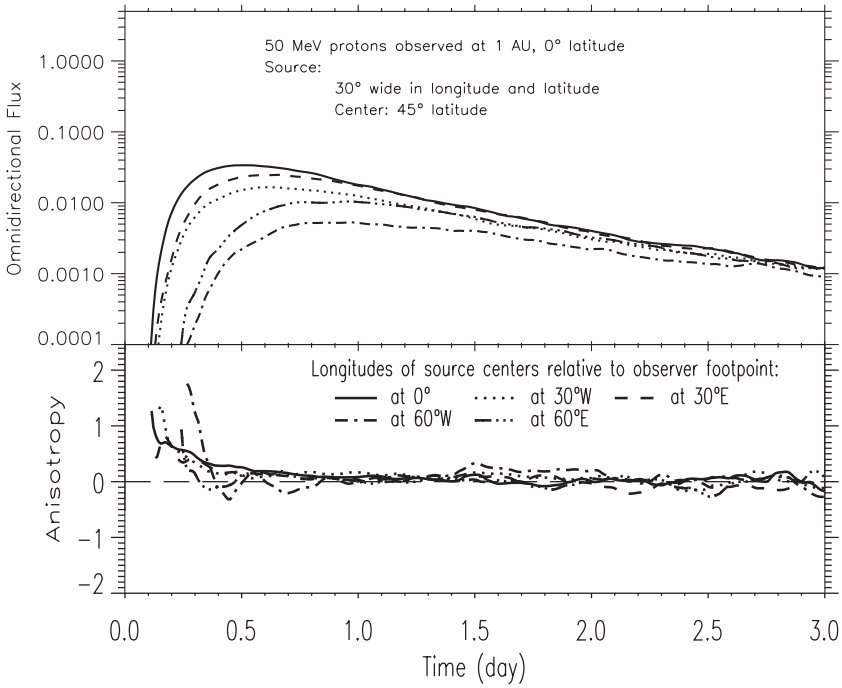

Figure 3. Same as Figure 2, except that the center of particle sources is moved to 45° latitude.

footpoint of the observer than those when the sources are located west, and the times of onset and maximum flux are earlier, too.

When the observer is connected directly to the solar source by the IMF footpoint, the first-order anisotropy is larger than that during the rising phase. We can also see that when the longitude separation between the IMF footpoint of the observer and source is large, e.g., 60° away in longitude, either west or east, the anisotropy can be negative during the early rising phase of the SEP flux. This indicates that the first arriving particles are mostly moving toward the Sun. Both the negative and positive anisotropies decrease as the event evolves. Two days after the onset of the SEP event, all the anisotropy profiles reach about 0. This means that the particles become nearly isotropic in pitch-angle distribution during the late phase.

Figure 3 shows a comparison of simulations similar to those in Figure 2, the only difference is that now the source centers are located at 45° latitude. The observer is not connected to any of the sources due to the difference in latitude. The SEP omnidirectional flux is the largest when the source is the nearest to the observer footpoint, i.e., when both the source and the IMF footpoint of the observer are at the same longitude. The farther the IMF footpoint of the observer is away from the source, the

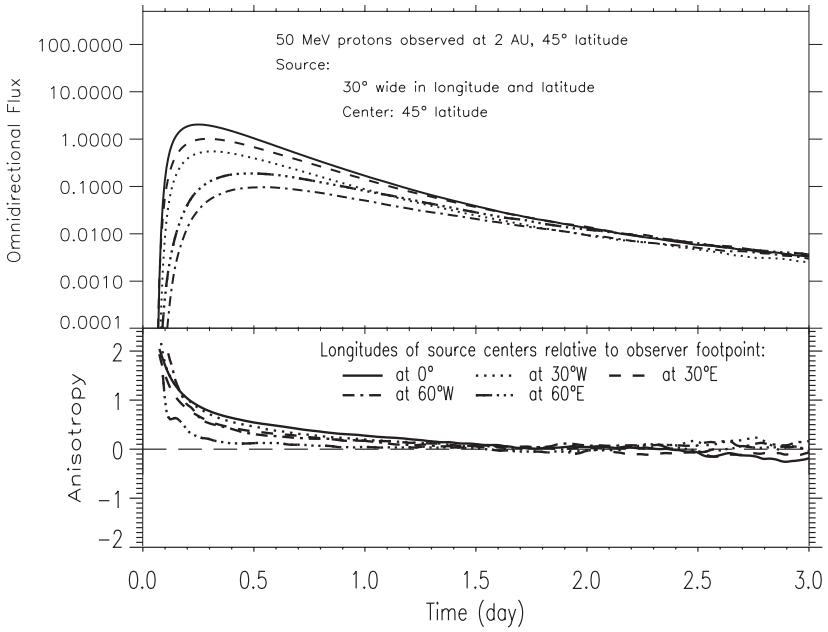

Figure 4. Omnidirectional flux and anisotropy of 50 MeV protons observed at 2 AU, 45° latitude. Different line styles indicate different distances in longitude between the IMF footpoint of the observer and the center of particle sources on the Sun. All the sources are located at 45° latitude and have a 30° coverage in both latitude and longitude.

smaller the particle flux observed will be, and also the later the event arrives. With the same separation in longitude from the IMF footpoint of the observer to the source centers, the SEPs with the sources located east are detected earlier with larger fluxes than those with the sources located west. Because in all the cases in this figure the observer footpoint is farther away from sources than those in Figure 2, the fluxes in this figure are smaller.

The anisotropies in Figure 3 are all positive at the onset of flux and decrease toward the value 0 after the first arrival of SEPs. About half a day after the onset of the SEP flux, all the anisotropies become 0 and remain so during the late phase of the SEP event.

Figure 4 shows another comparison of simulations similar to those in Figure 3, i.e., the centers of sources are located at 45° latitude; however, now the observer is located at 2 AU, 45° latitude. As we can see, when the source is directly connected to the observer by the IMF line the flux is larger than that when the sources are not connected. The further the IMF footpoint of the observer is away from the source, the smaller the particle flux observed is, and also the later the flux increase arrives. As in the previous cases, with the same separation in longitude between the IMF footpoint of the observer and the source centers, the events with sources located east are detected earlier with larger fluxes than those with the sources located west. About two days after the onset, all the five fluxes reach almost the same level, which is consistent with the picture depicted by the SEP reservoir phenomenon. The formation of SEP reservoir mainly comes from the effect of perpendicular diffusion (Zhang et al. 2009). The anisotropy profiles in Figure 4 behave similarly to those in Figure 3.

Figure 5 shows a comparison of simulations similar to those in Figure 4, the only difference is that now the centers of sources are located at 0° latitude. They also are similar to those in Figure 2, but now the observer is at 2 AU, 45° latitude. The flux profiles in Figure 5 are similar to all previous cases, but the levels are lower since the footpoint of the observer is farther away from the sources.

The anisotropy profiles for those cases in Figure 5 behave quite differently from all the previous cases. When the longitude of source centers relative to the observer footpoint is at 0°, 30° W, 30° E, and 60° E, respectively, anisotropies start with positive maximum values at the onset; then they decrease as more particles arrive later. However, for the case where the longitude of the source center relative to the observer footpoint is at 60° W, the anisotropy has a very negative value at first, and then its magnitude decreases toward 0 afterward.

To directly compare absolute intensities and shapes of time profiles between the figures above, a summary (Figure 6) of Figures 2, 3, 4, and 5 that just includes the 0° line for each run is provided. From the top panel of Figure 6, we can see, when the observer and source center are at 0° latitude, the onset and the peak of the SEP flux are detected the earliest, and throughout the entire phase, the flux intensity is the largest. When the observer and source center are at 45° latitude, the onset and the peak of SEP flux are detected the second earliest, and throughout the entire phase, the flux intensity is the second largest. The onset and the peak of SEP flux are detected late and the flux intensity is small when the observer and source latitudes are separated by 45°.

3.2. The Effect of Source Coverage in Latitude and Longitude

Figure 7 shows a comparison of simulations with different source coverages in latitude and longitude. It shows the results of simulations for 50 MeV protons as observed at 1 AU, 0° latitude when the observer is connected to the sources by the IMF lines. The upper and lower panels are the SEP omnidirectional flux and anisotropy, respectively. We put the center of the solar particle source at the IMF footpoint of the observer. The widths of the latitude and longitude coverage for these sources are 30°, 45°, 60°, 75°, and 90° as shown by different line styles.

From the top panel of Figure 7, we can see, for all the five cases, the observer detects the onset and the peak of SEP flux

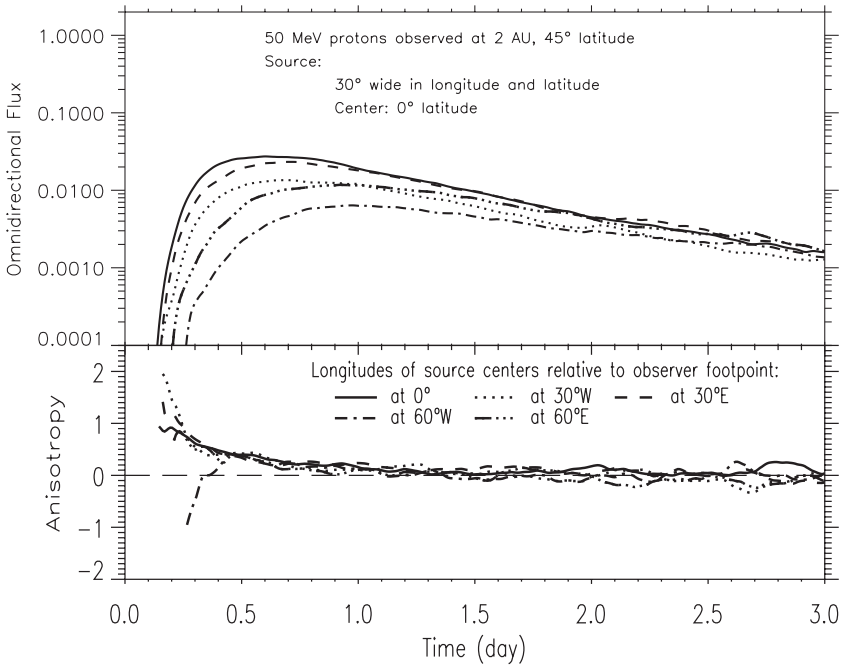

Figure 5. Same as Figure 4, except that the center of particle sources is moved to the equator or 0° latitude.

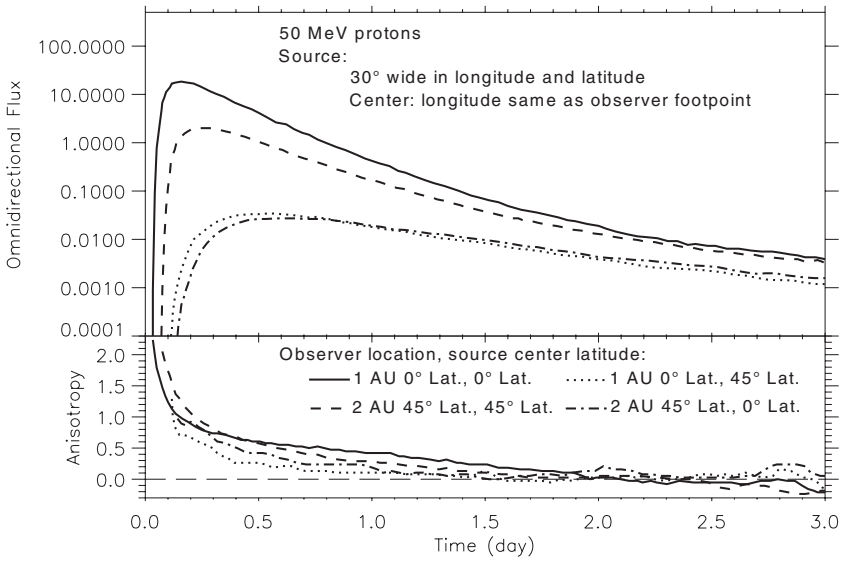

Figure 6. Summary of Figures 2, 3, 4, and 5 that just includes the 0° line for each run.

at about the same time. In this work, we define the decay rate as the gradient in the decreasing phase of the line in the figure, i.e., $(\lg F_2 - \lg F_1)/(t_2 - t_1)$ for the flux profiles, and $(A_2 - A_1)/(t_2 - t_1)$ for the anisotropy profiles. After the peak time, the five flux profiles decrease in time with different decay rates. Specifically, the decay becomes faster as the source width decreases from 90° to 30°.

In the lower panel of Figure 7, all the anisotropy profiles decrease toward the value of 0 from their initial positive maximum value. At the beginning, the five anisotropy profiles have almost the same decay rate. Later on, the anisotropy with a larger source width decreases more rapidly. All the five anisotropy profiles become nearly 0 two days after the onset, which means that all the particles have become isotropic by that time.

Figure 8 shows a comparison of simulations similar to those in Figure 7. The only difference is that now the observer is at 2 AU, 45° latitude. The center of the particle source is still located at the IMF footpoint of the observer. The flux profiles of the five cases have about the same onset time, peak time, and decay rate in the decay phase. However, the cases with wider sources have larger fluxes. At the same time the five anisotropy profiles decrease from positive maximum values. The decay rate of particle anisotropy is larger for the cases with larger source widths.

Figure 9 shows a comparison of simulations similar to those in Figure 7, but now the center of those sources is located at 45° latitude. The particle sources are not connected to the observer by the IMF lines. We can see that the events with larger source widths appear earlier and their peak fluxes are also

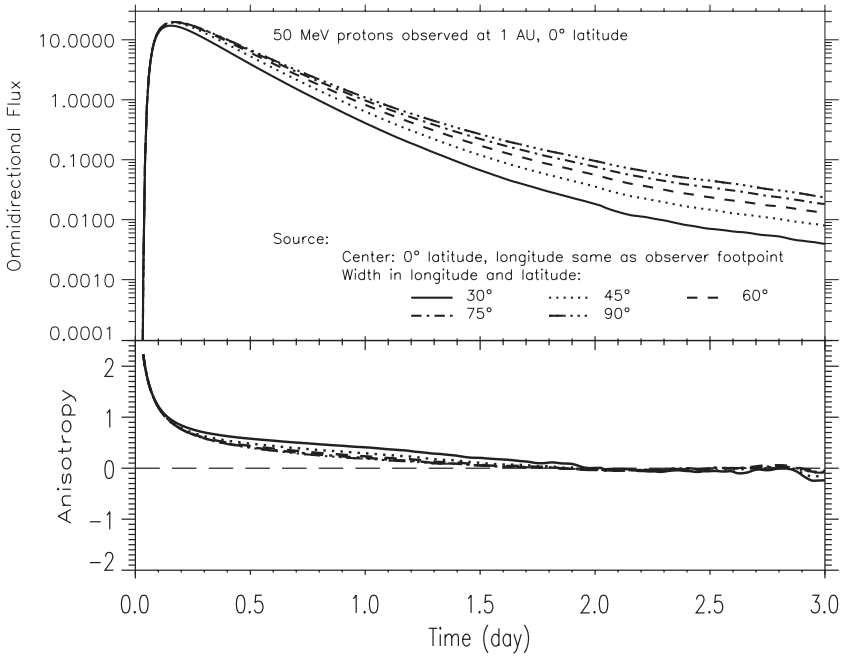

Figure 7. Omnidirectional flux and anisotropy of 50 MeV protons observed at 1 AU, 0° latitude. The source centers are at the IMF footpoint of the observer. Different line styles indicate different widths of source coverage in longitude and latitude.

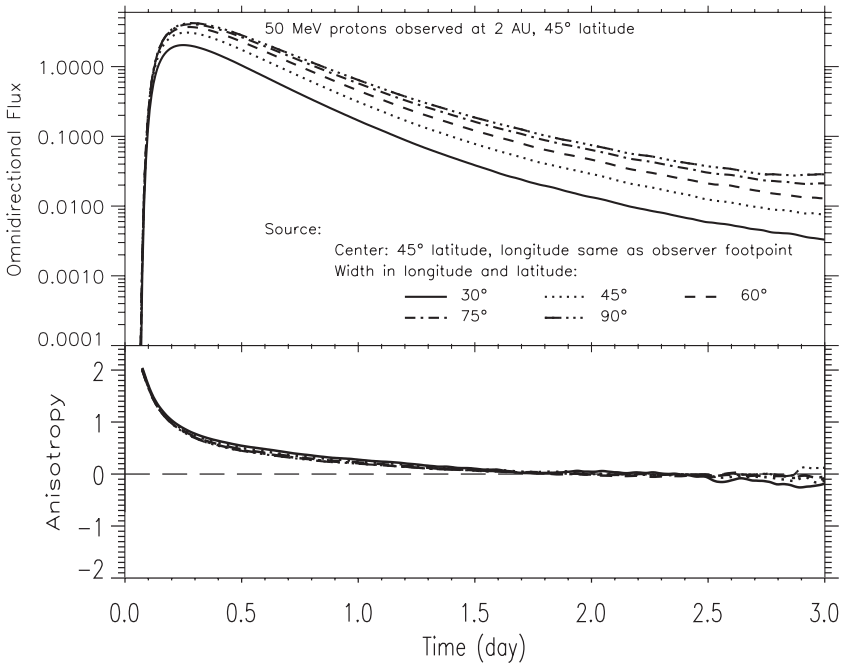

Figure 8. Omnidirectional flux and anisotropy of 50 MeV protons observed at 2 AU, 45° latitude. The source centers are at the IMF footpoint of the observer. Different line styles indicate different widths in longitude and latitude of sources.

higher. The profiles of anisotropy behave regularly. All start with some positive values and then decay to 0 afterward.

Figure 10 shows another comparison of simulations similar to those in Figure 8, but now the source centers are located at 0° latitude. The SEP sources are not connected to the observer with IMF lines. The flux and anisotropy profiles are similar to those in Figure 9 except that the differences between the cases with different source widths are more prominent in Figure 9. This is mainly an effect of radial distance.

3.3. The Effect of Source Spatial Variation

In this part, we study the effect of the spatial variation of the particle injection strength inside the source region on the propagation of SEPs in the three-dimensional IMF. We choose the following five different spatial variation functions for the source $a(\theta, \phi)$ as a function of latitude and longitude (θ, ϕ) in Equation (8): (1) cosine function, $a(\theta, \phi) = a_0 \cos \psi$; (2) tangent function, $a(\theta, \phi) = a_0 \tan(\pi/3 - \psi)$; (3) exponential function, $a(\theta, \phi) = a_0 e^{-\psi}$; (4) polynomial function, $a(\theta, \phi) =$

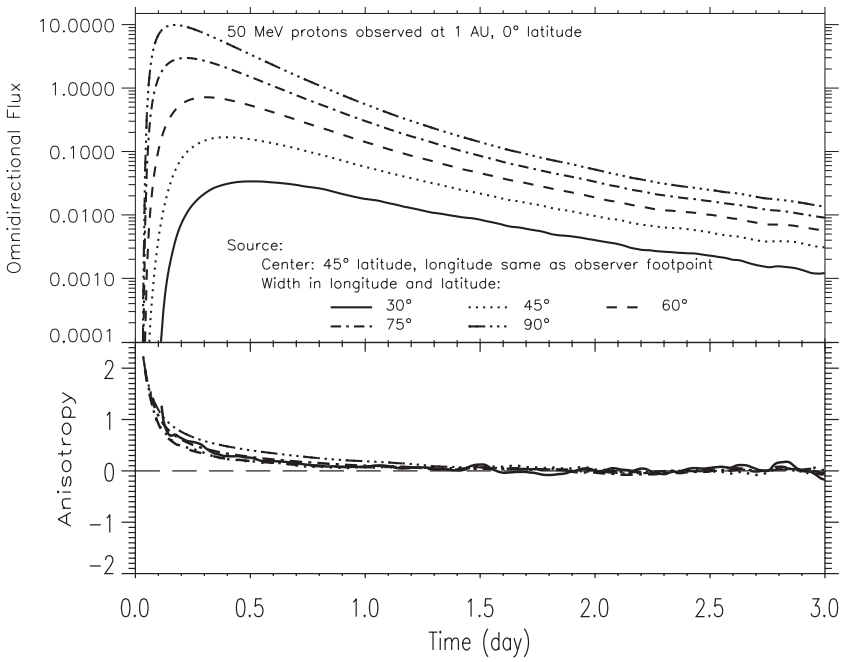

Figure 9. Same as Figure 7, except that the center of particle sources is moved to 45° latitude.

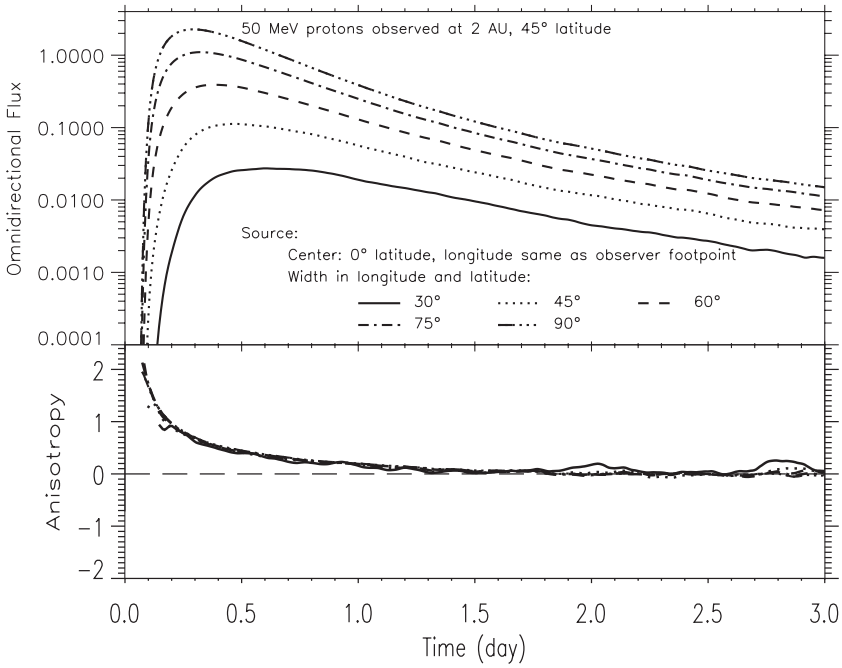

Figure 10. Same as Figure 8, except that the center of particle sources is moved to the equator or 0° latitude.

$a_0(3.3 - \psi - \psi^2 - \psi^3)$; and (5) Gauss distribution function, $a(\theta, \phi) = a_0 e^{-\psi^2/2}$. The constant a_0 is normalized according to the formula defined by Equation (9) so that the total source particle injection remains the same in all these spatial injection profiles. In the above functions,

$$\cos\psi = \sin\theta_0 \sin\theta + \cos\theta_0 \cos\theta \cos(\phi_0 - \phi), \qquad (11)$$

where ψ denotes the angular distance between any location (θ, ϕ) at the source and the source center denoted by the heliospheric latitude and longitude (θ_0, ϕ_0).

Figure 11 shows a comparison of simulations for the 50 MeV protons as detected at 1 AU, 0° latitude with those different source spatial variations. All source regions extend 90° from the center. The top panel shows the source spatial variation $a(\theta, \phi)$ as a function of the angular distance ψ. The middle and bottom panels show the SEPs' omnidirectional flux and anisotropy at 1 AU. From the figure, we can see that in all the events the flux and anisotropy profiles are almost the same. We have also studied the effect of the spatial variation of the source function on the flux and anisotropy observed at other locations. The results are basically similar to those shown in Figure 11. Therefore, we can conclude that the details of the spatial variation of the source function needed in Equation (8) usually do not affect the flux and anisotropy profiles very much, unless the source distribution

Table 1
Summary Table of All the Cases in the Figures, Including the Simulation Parameters (Source Latitude, Source Width, Observer Location, Longitude Distance Between Source Center and Observer Footpoint, Spatial Variation Function) and the Result Parameters (Onset Time, Peak Flux, Peak Flux Time, Decay Rate)

Figure No.	Source	Width	Observer	Distance	Function	Onset (day)	Peak	Peak Time (day)	Decay Rate	
									Flux	Aniso.
				0°		0.03	16	0.13	−1.24	−1.73
				30° W		0.04	1	0.26	−0.88	−2.08
2	0° Lat.	30°	1 AU, 0° Lat.	30° E	Uniform	0.035	1.5	0.25	−0.94	−1.77
				60° W		0.15	0.07	0.69	−0.59	0.24
				60° E		0.12	0.13	0.58	−0.62	1.27
				0°		0.11	0.033	0.5	−0.59	−1.28
				30° W		0.14	0.016	0.62	−0.49	−1.34
3	45° Lat.	30°	1 AU, 0° Lat.	30° E	Uniform	0.13	0.024	0.6	−0.56	−0.98
				60° W		0.26	0.005	0.9	−0.35	−2.36
				60° E		0.24	0.01	0.8	−0.44	−1.22
				0°		0.06	2.1	0.23	−1.00	−1.89
				30° W		0.07	0.5	0.31	−0.83	−2.13
4	45° Lat.	30°	2 AU, 45° Lat.	30° E	Uniform	0.06	1	0.3	−0.92	−1.84
				60° W		0.11	0.1	0.52	−0.60	−1.94
				60° E		0.09	0.2	0.46	−0.68	−1.59
				0°		0.14	0.028	0.6	−0.52	−0.88
				30° W		0.15	0.015	0.72	−0.47	−2.23
5	0° Lat.	30°	2 AU, 45° Lat.	30° E	Uniform	0.15	0.023	0.72	−0.50	−1.33
				60° W		0.26	0.0068	1.02	−0.35	1.42
				60° E		0.21	0.012	0.98	−0.42	−0.95
		30°				0.03	18	0.17	−1.29	−1.79
		45°				0.03	19	0.17	−1.19	−1.96
7	0° Lat.	60°	1 AU, 0° Lat.	0°	Uniform	0.03	20	0.17	−1.11	−2.02
		75°				0.03	20	0.17	−1.07	−2.08
		90°				0.03	20	0.17	−1.03	−2.09
		30°				0.07	2	0.24	−1.01	−1.78
		45°				0.07	3	0.24	−0.94	−1.85
8	45° Lat.	60°	2 AU, 45° Lat.	0°	Uniform	0.07	3.8	0.24	−0.88	−1.96
		75°				0.07	4	0.24	−0.83	−1.96
		90°				0.07	4.2	0.24	−0.78	−1.96
		30°				0.11	0.035	0.5	−0.59	−1.31
		45°				0.06	0.18	0.4	−0.68	−1.70
9	45° Lat.	60°	1 AU, 0° Lat.	0°	Uniform	0.04	0.73	0.3	−0.77	−1.70
		75°				0.03	3	0.21	−0.90	−1.69
		90°				0.03	10	0.16	−0.99	−1.57
		30°				0.14	0.028	0.6	−0.51	−0.84
		45°				0.09	0.11	0.45	−0.56	−1.12
10	0° Lat.	60°	2 AU, 45° Lat.	0°	Uniform	0.08	0.4	0.37	−0.66	−1.76
		75°				0.07	1.1	0.3	−0.73	−1.96
		90°				0.07	2.3	0.26	−0.79	−1.96
					$\cos\psi$	0.03	8	0.17	−1.04	−2.02
					$\tan(\pi/3-\psi)$	0.03	10	0.17	−1.09	−1.97
11	0° Lat.	90°	1 AU, 0° Lat.	0°	$e^{-\psi}$	0.03	9	0.17	−1.06	−2.00
					$3.3-\psi-\psi^2-\psi^3$	0.03	9	0.17	−1.06	−2.00
					$e^{-\psi^2/2}$	0.03	9	0.17	−1.06	−2.00

is extremely ill-behaved, i.e., the spatial variation function is singular.

Finally, for direct comparison among all the cases in the figures, we show the simulation parameters (source latitude, source width, observer location, longitude distance between source center and observer footpoint, spatial variation function) and the result parameters (onset time, peak flux, peak flux time, decay rate) in Table 1.

4. SUMMARY

We have studied SEP propagation in the three-dimensional Parker interplanetary magnetic field by numerically solving the focused transport equation with perpendicular diffusion. We have investigated how the source locations, coverage of latitude and longitude, and spatial variations will affect the observations of SEP flux and anisotropy time profiles at different locations in heliosphere. The following are the main conclusions of our results in this paper.

1. Perpendicular diffusion mechanism plays a very important role in SEP propagation. It can be used to explain many observational phenomena, particularly when a spacecraft is not directly connected to the solar source by the IMF lines.
2. The location of SEP source has the greatest effects on the observed SEP flux and anisotropy profiles. The farther the IMF footpoint of the observer is away from the source, the smaller the particle flux observed will be, and the

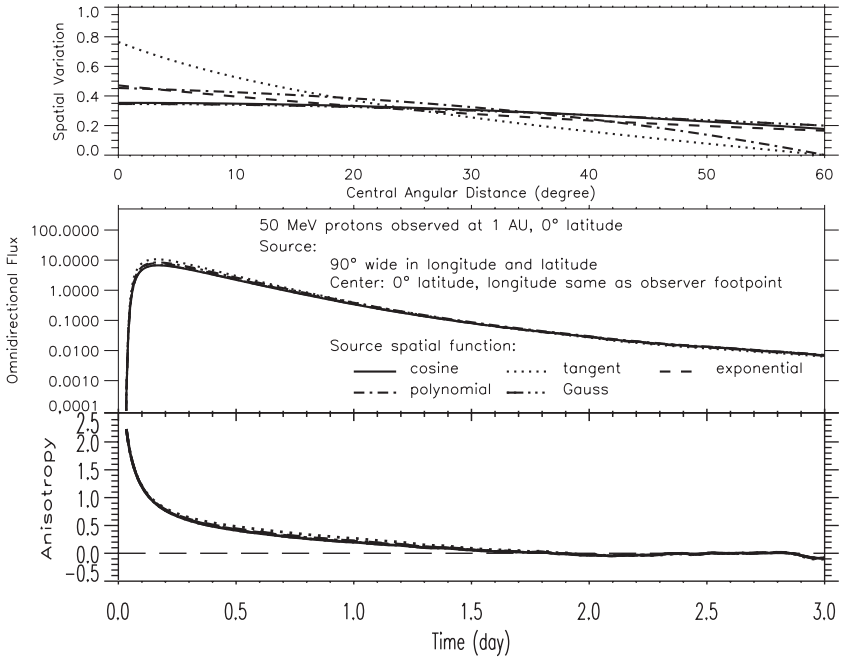

Figure 11. Omnidirectional flux and anisotropy of 50 MeV protons observed at 1 AU, 0° latitude. The sources are 90° wide and centered at the IMF footpoint of the observer. Different line styles correspond to different functions for the spatial distribution of particle intensity inside the sources.

later the onset and the peak of SEP flux will appear. Particles from a source on the east side or west side relative to the footpoint of the spacecraft will appear differently, even though the longitudinal separation and other source characteristics are the same. This effect results from the azimuthal asymmetry of the Parker interplanetary magnetic field. When the IMF footpoint of the observer is very far away from the source in longitude, e.g., by as much as 60°, the first arriving SEPs could be moving toward the Sun. These are the particles that first stream out along field lines to large radial distances, diffuse across field lines onto the line that connects the observer, get scattered in the pitch angle, and then return to the observer from outside.

3. The coverage of the source in latitude and longitude also has large effects on the SEP flux and anisotropy profiles. Particles coming from a wider source tend to have large fluxes. When the IMF footpoint of the observer is at the centers of the SEP sources, the onset and the peak fluxes are almost the same for sources of different coverages in longitude and latitude. However, when the IMF footpoint of the observer is not located inside the source region, a wider source coverage will result in an earlier onset and peak flux.
4. The flux and anisotropy profiles in the cases with different normalized spatial variations of SEP source injection appear almost the same if all the other conditions remain the same. It indicates that the form of the spatial variation is not very important in affecting the SEP flux and anisotropy, unless its distribution is extremely strange.

We are grateful to National Natural Science Foundation of China for partial support under grants NNSFC 41074125 and 40921063, CMA grant GYHY201106011, and National High-tech R&D Program of China (863 Program) under grant 2010AA122200. M.Z. was supported in part by NASA under grant NNX08AP91G.

REFERENCES

Beeck, J., & Wibberenz, G. 1986, ApJ, 311, 437
Bieber, J. W., Matthaeus, W. H., Shalchi, A., & Qin, G. 2004, Geophys. Res. Lett., 31, L10805
Bieber, J. W., Matthaeus, W. H., Smith, C. W., Wanner, W., Kallenrode, M.-B., & Wibberenz, G. 1994, ApJ, 420, 294
Cane, H. V., Reames, D. V., & von Rosenvinge, T. T. 1988, J. Geophys. Res., 93, 9555
Droge, W. 1994, ApJS, 90, 567
Dwyer, J. R., et al. 1997, ApJ, 490, L115
Earl, J. A. 1974, ApJ, 193, 231
Earl, J. A. 1976, ApJ, 205, 900
Giacalone, J., & Neugebauer, M. 2008, ApJ, 673, 629
Hasselmann, K., & Wibberenz, G. 1968, Z. Geophys., 34, 353
Hasselmann, K., & Wibberenz, G. 1970, ApJ, 162, 1049
He, H.-Q., & Qin, G. 2011, ApJ, 730, 46
Hundhausen, A. J. 1993, J. Geophys. Res., 98, 13177
Hurford, G. J., Krucker, S., Lin, R. P., Schwartz, R. A., Share, G. H., & Smith, D. M. 2006, ApJ, 644, L93
Isenberg, P. A. 1997, J. Geophys. Res., 102, 4719
Jokipii, J. R. 1966, ApJ, 146, 480
Kóta, J., & Jokipii, J. R. 1997, in Proc. 25th ICRC, 1, 213
Lario, D., et al. 2003, Adv. Space Res., 32, 579
Li, G., Zank, G. P., & Rice, W. K. M. 2003, J. Geophys. Res., 108, SSH 10-1
Maclennan, C. G., Lanzerotti, L. J., & Gold, R. E. 2001, Space Sci. Rev., 97, 281
Maia, D., Pick, M., Hawkins, S. E., III, Fomichev, V. V., & Jiřička, K. 2001, Sol. Phys., 204, 199
Matthaeus, W. H., Qin, G., Bieber, J. W., & Zank, G. P. 2003, ApJ, 590, L53
McKibben, R. B. 1972, J. Geophys. Res., 77, 3957
McKibben, R. B., et al. 2003, Ann. Geophys., 21, 1217
Parker, E. N. 1963, Interplanetary Dynamic Processes (New York: Interscience)
Qin, G. 2002, PhD thesis, Univ. Delaware
Qin, G. 2007, ApJ, 656, 217
Qin, G., Matthaeus, W. H., & Bieber, J. W. 2002, ApJ, 578, L117
Qin, G., & Shalchi, A. 2009, ApJ, 707, 61
Qin, G., Zhang, M., & Dwyer, J. R. 2006, J. Geophys. Res., 111, A08101
Qin, G., Zhang, M., Dwyer, J. R., & Rassoul, H. K. 2004, ApJ, 609, 1076
Qin, G., Zhang, M., Dwyer, J. R., Rassoul, H. K., & Mason, G. M. 2005, ApJ, 627, 562
Reames, D. V. 1999, Space Sci. Rev., 90, 413
Reames, D. V., Kahler, S. W., & Ng, C. K. 1997, ApJ, 491, 414
Reid, G. C. 1964, J. Geophys. Res., 69, 2659

Roelof, E. C. 1969, in Lectures in High Energy Astrophysics, ed. H. Ogelmann & J. R. Wayland (NASA SP-199; Washington, DC: NASA), 111
Roelof, E. C., Gold, R. E., Simnett, G. M., Tappin, S. J., Armstrong, T. P., & Lanzerotti, L. J. 1992, Geophys. Res. Lett., 19, 1243
Ruffolo, D. 1995, ApJ, 442, 861
Schlickeiser, R. 2002, Cosmic Ray Astrophysics (Berlin: Springer)
Shalchi, A., Bieber, J. W., Matthaeus, W. H., & Qin, G. 2004, ApJ, 616, 617
Skilling, J. 1971, ApJ, 170, 265
Tan, L. C., Reames, D. V., Ng, C. K., Saloniemi, O., & Wang, L. 2009, ApJ, 701, 1753
Wang, Y.-M., Pick, M., & Mason, G. M. 2006, ApJ, 639, 495
Zank, G. P., Rice, W. K. M., & Wu, C. C. 2000, J. Geophys. Res., 105, 25079
Zhang, M. 1999, ApJ, 513, 409
Zhang, M., Jokipii, J. R., & McKibben, R. B. 2003, ApJ, 595, 493
Zhang, M., Qin, G., & Rassoul, H. 2009, ApJ, 692, 109